Available online at www.sciencedirect.com
SCIENCE DIRECT®
Journal of volcanology and geothermal research
ELSEVIER
Journal of Volcanology and Geothermal Research 153 (2006) 148–165
www.elsevier.com/locate/jvolgeores

From Vulcanian explosions to sustained explosive eruptions: The role of diffusive mass transfer in conduit flow dynamics

R.M. Mason [a], A.B. Starostin [a,*], O.E. Melnik [a,b], R.S.J. Sparks [a]

[a] *Earth Science Department, Wills Memorial Building University of Bristol, Queen's Road, Bristol BS81RJ, UK*
[b] *Institute of Mechanics, Moscow State University, 1-Michurinskii prosp., Moscow 117192, Russia*

Received 31 March 2004; accepted 17 August 2005
Available online 3 February 2006

Abstract

Magmatic explosive eruptions are influenced by mass transfer processes of gas diffusion into bubbles caused by decompression. Melnik and Sparks [Melnik, O.E., Sparks, R.S.J. 2002, Modelling of conduit flow dynamic during explosive activity at Soufriere Hills Volcano, Montserrat. In: Druitt, T.H., Kokelaar, B.P. (eds). The Eruption of Soufriere Hills Volcano, Montserrat, from 1995 to 1999. Geological Society, London, Memoirs, 21, 307–317] proposed two end member cases corresponding to complete equilibrium and complete disequilibrium. In the first case, diffusion is fast enough to maintain the system near equilibrium and a long-lived explosive eruption develops. In the latter case, pre-existing bubbles expand under conditions of explosive eruption and decompression, but diffusive gas transfer is negligible. This leads to a much shorter eruption. Here we develop this model to consider the role of mass transfer by investigating transient flows at the start of an explosive eruption triggered by a sudden decompression. The simulations reveal a spectrum of behaviours from sustained to short-lived highly non-equilibrium Vulcanian-style explosions lasting a few tens of seconds, through longer lasting eruptions that can be sustained for tens of minutes and finally to eruptions that can last hours or even days. Behaviour is controlled by a mass-transfer parameter, ω, which equals $n_*^{2/3}D$, where n_* is the bubble number density and D is the diffusivity. The parameter ω is expected to vary between 10^{-5} and 1 s^{-1} in nature and reflects a time-scale for efficient diffusion. The spectrum of model behaviours is consistent with variations in styles of explosive eruptions of silicic volcanoes. In the initial stages peak discharges occur over 10–20 s and then decline to low discharges. If a critical bubble overpressure is assumed to be the criterion for fragmentation then fragmentation may stop and start several times in the declining period causing several pulses of high-intensity discharge. For the cases of strong disequilibria, the fluxes can decrease to negligible values where other processes, such as gas escape through permeable magma, prevents explosive conditions becoming re-established so that explosive activity stops and dome growth can start. For cases closer to the equilibrium the eruption can evolve towards a quasi-steady sustained flow, never declining sufficiently for gas escape to become dominant.

Keywords: explosive eruption; extrusion; fragmentation; diffusion

1. Introduction

The dynamics of explosive volcanic eruptions can be usefully investigated by mathematical models. Conduit flows involve the transition from slow ascent of bubbly viscous magma through a fragmentation zone to a high-speed flow of a gas-particle dispersion (Fig. 1). Math-

* Corresponding author. Institute of Mechanics, Moscow State University, 1-Michurinskii prosp., Moscow 117192, Russia. Tel.: +7 495 939 52 86; fax: +7 495 939 01 65.
E-mail address: starab@yandex.ru (A.B. Starostin).

0377-0273/$ - see front matter © 2005 Elsevier B.V. All rights reserved.
doi:10.1016/j.jvolgeores.2005.08.011

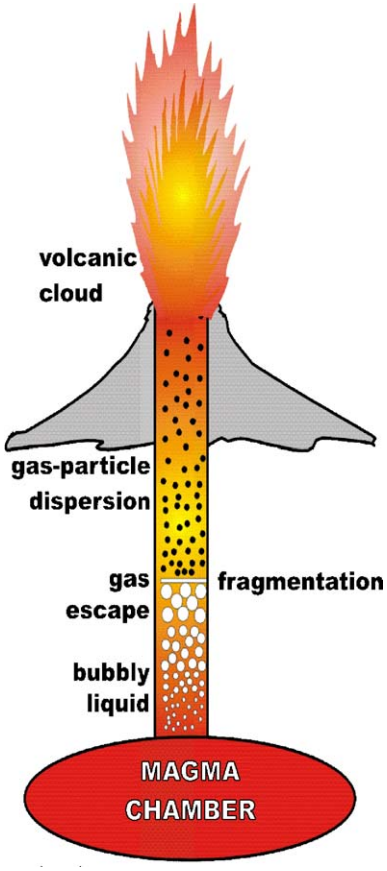

Fig. 1. Schematic representation of flow zones during explosive eruptions. Magma undergoes the instantaneous nucleation, zone with gas exsolution into the bubbles and possible gas escape, then abrupt fragmentation and zone of gas-particle dispersion.

ematical descriptions of these flows involve making various assumptions about the properties of the magma, the boundary conditions, and the geometry of the volcanic system. This paper considers three main related issues. First, there is the question of how close explosive flows are to conditions of equilibrium between dissolved and exsolved gas. Second, there is the issue whether the activity consists of a short-lived Vulcanian explosion or develops into a sustained, long-lived Plinian style eruption. Melnik and Sparks (2002a,b) proposed that these contrasted styles might be controlled by the extent of disequilibrium. Third, there is the issue of the initial evolution of explosive eruptions from unsteady to quasi-steady flows.

A central matter is the extent to which the gas exsolution is at equilibrium during the processes of bubble nucleation and growth in explosive conduit flows. The possibility of strong disequilibrium and large supersaturations were recognised by Proussevitch and Sahagian (1996), Navon and Lyakhovsky (1998), and Mangan and Sisson (2001). Decompression rates may be so fast that bubble growth occurs far from equilibrium (Gardner et al., 2000). Two end member cases may be recognized when a column of a gas-rich magma is decompressed and an explosive flow initiates (Melnik and Sparks, 2002a). In one the system is always maintained close to equilibrium and the flow expands continuously. In the complete disequilibrium end member the existing bubbles in the column expand, but there is negligible diffusion into these bubbles and no extra nucleation occurs. The first case may correspond to sustained long-lived Plinian eruptions and the later case may correspond to short-lived Vulcanian eruptions where the explosive flow stops because there is only a finite amount of bubbly magma that can expand to reach critical conditions for fragmentation.

The majority of conduit flow models have investigated the quasi-steady, sustained flows that develop once an eruption has become well established (Wilson et al., 1980; Papale and Dobran, 1993; Papale, 1999; Melnik, 2000; Slezin, 2003). In this situation an approximate balance is achieved between the flow regimes in the conduit (Fig. 1) and parameters change sufficiently slowly so that the fragmentation level adjusts to maintain quasi-steady flow condition. This situation is not appropriate for the early stages of explosive eruptions due to a sudden decompression induced, for example, by dome or sector collapse. Our investigation focuses on such unsteady initial flows and how they can adjust to quasi-steady conditions.

This paper develops the model of Melnik and Sparks (2002a) to investigate the role of gas diffusion in transient explosive volcanic flows. The two end members, studied by Melnik and Sparks (2002a), correspond to fast diffusion in decompressing magma and slow diffusion where negligible gas is transferred into expanding gas bubbles during the decompression. Here fast and slow diffusion terms are used relative to the time scale for the magma decompression in explosive conduit flows. By introducing diffusion into the problem, we can investigate under what conditions the two end-member cases might be good approximations. We also compare different fragmentation assumptions, namely, fragmentation at a fixed volume fraction of bubbles (Sparks, 1978; Wilson et al., 1980) and fragmentation at a fixed overpressure in growing bubbles (Barmin and Melnik, 1993; Melnik, 2000). Our model is concerned with the initial stage of explosive eruption when the column of slowly ascending magma is suddenly decompressed and the pressure reduction is sufficient

to reach conditions for explosive fragmentation. Such an initiating event might be a dome collapse, a sector collapse or simply development of an excess pressure at the top of the conduit that reaches the fragmentation threshold. The evolution of initial unsteady flow depends on the physical conditions in the magma column before an eruption is triggered, so we also develop a model of a slow magma ascent that sets up the initial conditions for explosive flows. We finally investigate how initial unsteady flows might evolve into sustained quasi-steady flows.

2. The model

2.1. Description of the physical system

Active silicic volcanoes are commonly in the state of slow magma ascent which feeds either lava domes or intrusive cryptodomes. The conduit is filled with magma which ascends slowly and decompresses, resulting in nucleation and growth of bubbles driven by diffusion of the gas from the melt. Near the surface gas can escape through permeable magma all the way to the surface or the conduit wallrocks (Taylor et al., 1983; Woods and Koyaguchi, 1994; Jaupart, 1998; Melnik and Sparks, 1999; Melnik and Sparks, 2002b). The extruding dome or cryptodome maintains a pressure difference between the magma ascending in the conduit and atmosphere, which can be related to variations in dome height and degassing processes that cause rheological stiffening (Stasiuk and Jaupart, 1997; Melnik and Sparks, 1999). To describe the dynamics of a slow extrusion, we develop a steady model.

Lava dome extrusion or cryptodome intrusion can turn to explosive eruption by a sudden decompression. A common cause of a sudden decompression is dome collapse, as at the Soufriere volcano, Montserrat (Robertson et al., 1998; Druitt et al., 2002) and edifice collapse, as at Mount St. Helens (Voight et al., 1981). After collapse the pressure at the top of the conduit decreases rapidly. A rarefaction wave propagates down the conduit reducing the pressure. Bubbles in the magma respond to the pressure change by expanding, but viscous resistance result in excess pressure. If this overpressure exceeds a critical threshold for fragmentation, then explosive disruption can initiate. Alternatively the bubble can grow to reach a critical volume fraction of bubbles for fragmentation. In both cases the fragmentation occurs in a zone of small length in comparison with the length of the conduit (Barmin and Melnik, 1993). Fragmented bubbly liquid forms a gas-particle dispersion.

The fragmentation front propagates down following the rarefaction wave and the gas-particle dispersion zone expands. In this zone material accelerates easily as the viscosity is negligible. To describe the dynamics of an explosive eruption, which is triggered by a sudden decompression, we develop an unsteady model.

2.2. Governing equations

The mechanical description of conduit flow during explosive eruptions has been extensively discussed in Wilson et al. (1980), Dobran (1992), Barmin and Melnik (1993), Woods and Koyaguchi (1994), Papale (1999), Melnik (2000), Melnik and Sparks (2002a), Slezin (2003). The present model develops the models of Melnik and Sparks (2002a), where two end-member cases were considered; one in which diffusion into the growing bubbles is fast enough to maintain the system close to equilibrium and the other in which diffusion is so slow that bubbles that existed prior to the onset of explosive activity expand without further significant mass transfer. Dimensional analysis provides criteria for these cases based on the Peclet number, Pe, which is the ratio of the characteristic time of diffusion of dissolved gas and the characteristic time of decompression (Navon and Lyakhovsky, 1998). In one end member case ($Pe \gg 1$) the mass transfer between the melt and bubbles is negligible. This might be reasonable for the initial stages of an explosive eruption when the fragmentation front has a velocity, V_f, typically in the range of tens to over 100 m/s (Spieler et al., 2004). In the second end member case ($Pe \ll 1$) diffusion maintains the system close to equilibrium. This case describes a situation when the velocity of the fragmentation wave is sufficiently low that magma beneath the fragmentation front can grow bubbles close to equilibrium. Our goal is to establish when and if these end member situations might be applicable.

We consider the flow in the vertical conduit of a constant diameter. Our model excludes continuous nucleation, interaction of bubbles at high concentration, and variation of the mixture temperature (Barmin and Melnik, 1993). We assume that the relative velocities between bubbles and liquid and between particles and gas are small in comparison with the mixture velocity (Melnik, 2000). We also neglect changes in crystal content due to microlite crystallization (Melnik and Sparks, 2002a) as this process is very slow and is not expected to occur on the time scale of an explosive eruption. Because a mixture parcel spends a short time

in the zone of gas-particle dispersion, we neglect degassing in this zone. With these assumptions, the system of flow equations for both the bubbly liquid and gas-particle dispersion zones can be written as

$$\frac{\partial \rho}{\partial t} + \frac{\partial \rho v}{\partial x} = 0 \tag{1}$$

$$\frac{\partial \rho_e}{\partial t} + \frac{\partial \rho_e v}{\partial x} = \lambda J \tag{2}$$

$$\rho \frac{\partial v}{\partial t} + \rho v \frac{\partial v}{\partial x} = -\frac{\partial P}{\partial x} - \rho g - \lambda \frac{32 \mu_{av} v}{d^2} \tag{3}$$

$$\rho = \rho_e + \rho_d + \rho_m \tag{4}$$

$$P = \rho_e^0 R_w T \tag{5}$$

$$\rho_e = \alpha \rho_e^0 \tag{6}$$

$$\rho_m = (1-\alpha)\left[\beta \rho_x^0 + (1-\beta)(1-c_{av})\rho_m^0\right] \tag{7}$$

$$\rho_d = (1-\alpha)(1-\beta)c_{av}\rho_m^0 \tag{8}$$

Here and further, the following notations are used: ρ are densities (subscript: e, exsolved gas; d, dissolved gas; m, melt; x, crystal; no subscript, mixture; superscript: 0, pure; no superscript, reduced density, e.g., mass of a given component divided by unit volume of the mixture); d is the conduit diameter, v is the mixture velocity, P is the mixture pressure, α is the gas volume fraction per unit volume of mixture, β is the crystal content per unit volume of melt with crystals, T is the absolute magma temperature, R_w=461 J kg^{-1} K^{-1} is the gas constant divided by the molecular weight of water, t is the time and x is the vertical coordinate with x=0 corresponding to the top of the magma chamber and positive in the upward direction. The coefficient λ indicates the flow regime: λ=1 for bubbly liquid, and λ=0 for gas-particle dispersion. The subscript "av" relates to the dissolved water concentration, c, and viscosity, μ, averaged over the melt shells. The system consists of continuity equations for the mixture as a whole (1) and exsolved gas component (2), the momentum equation for the mixture as a whole (3), and equations of state (4)–(8). The continuity equations for exsolved gas component (2) accounts for a mass flux, J, due to diffusion. The momentum Eq. (3) takes into account gravity forces and conduit resistance (in Poiseuille form).

As we assume no bubble nucleation and no crystal growth the number density of bubbles per unit volume of magma, n, and density of the melt component are conserved in the parcel of magma:

$$\frac{\partial \rho_m}{\partial t} + \frac{\partial \rho_m v}{\partial x} = 0 \tag{9}$$

$$\frac{\partial n}{\partial t} + \frac{\partial n v}{\partial x} = 0 \tag{10}$$

The continuity Eqs. (9) and (10) can be integrated due to the assumption of equal component velocities (Melnik and Sparks, 2002a):

$$\frac{\rho_m}{\rho_{m*}} = \frac{n}{n_*} = \frac{\rho}{\rho_*} \tag{11}$$

$$\begin{aligned} \rho_* &= \beta \rho_x^0 + (1-\beta)\rho_m^0 \\ \rho_{m*} &= (1-\beta)(1-c_0)\rho_m^0 \end{aligned} \tag{12}$$

The subscript $_*$ relates to the values taken at the saturation pressure $P_*=(c_0/C_f)^2$ (Table 1), when $\alpha \ll 1$ and bubbles instantly nucleate with initial bubble number density n_*. Eqs. (4)–(11) allow calculation of P, α and n as functions of ρ and ρ_e. Neglecting c_{av} in comparison with 1 the integral (11) allows n to be expressed as

$$n = n_*(1-\alpha) \tag{13}$$

This equation takes account of the expansion of the parcel of magma so that the bubble number density per unit volume of magma reduces as the magma expands.

2.3. Diffusion of volatiles into bubbles

In order to describe diffusion, we use the quasi-steady bubble growth model of Lensky et al. (2001), which extends the shell model concept of Proussevitch et al. (1993) and Proussevitch and Sahagian (1996). For a solitary bubble, this growth model gives an exact distribution of volatiles concentration around the bubble. When there are many bubbles in the melt, we follow Proussevitch et al. (1993) in which each bubble is surrounded by a spherical shell of melt. The shell provides the bubble with water and expands according to mass conservation. Close to the bubble surface the water concentration is at equilibrium. Mass conservation of water inside the shell is used as a second boundary condition that allows to state the problem.

A diffusion equation with defining boundary conditions can be written as

$$\frac{dc}{dt} = \frac{\partial c}{\partial t} + \frac{\mathrm{d}r}{\mathrm{d}t}\frac{\partial c}{\partial r} = D\frac{1}{r^2}\frac{\partial}{\partial r}\left(r^2 \frac{\partial c}{\partial r}\right) \tag{14}$$

$$\frac{4}{3}\pi n a^3 = \alpha \quad \frac{4}{3}\pi n S^3 = 1 \tag{15}$$

$$c(a) = C_f\sqrt{P} \quad \frac{4}{3}\pi S_0^3 c_0 \rho_m^0 = \frac{4}{3}\pi a^3 \rho_e^0 + 4\pi\rho_m^0 \int_a^S r^2 c(r)\mathrm{d}r \tag{16}$$

Here c is the mass fraction of dissolved gas (water) in the melt, D is the diffusion coefficient of water in silicic melt, and C_f is the solubility coefficient. Eq. (15) relate the bubble radius a, the shell radius S, the number density per unit volume of magma and gas volume fraction n. We follow the concept of Proussevitch and Sahagian (1996) in approximation of the total volume of unfragmented magma column as the sum of all the shell volumes. Eq. (16) gives the boundary conditions for Eq. (14).

The mass flux, J, into a bubble is related to the concentration gradient on its border:

$$J = 4\pi a^2 n D \rho_m^0 \frac{\partial c}{\partial r}|_{r=a} \tag{17}$$

When Peclet number is small ($Pe \ll 1$) an approximate analytical solution can be written down, as the unsteady term in the diffusion Eq. (14) is negligibly small. Then concentration profile has a simple form (Lensky et al., 2001):

$$c(r) = C_1 + C_2\frac{1}{r} \tag{18}$$

The constants C_1 and C_2 can be found from Eqs. (14)–(16):

$$C_1 = \frac{2\rho_{g*}a^3 + \rho_{m*}\left(3c(a)a(S^2 - a^2) - 2c_0 S_0^3\right)}{\rho_{m*}(3S^2 a - a^3 - 2S^3)} \tag{19}$$

$$C_2 = \frac{2a\left(\rho_{g*}a^3 + \rho_{m*}\left(c(a)(S^3 - a^3) - c_0 S_0^3\right)\right)}{\rho_{m*}(3S^2 a - a^3 - 2S^3)} \tag{20}$$

$$\frac{4}{3}\pi n_* S_0^3 = 1 \qquad \rho_{g*} = c_0(1-\beta)\rho_m^0 \tag{21}$$

In order to apply this analytical solution (18) (19) (20) (21), we have to be sure that $Pe \ll 1$ in the conduit flow. However, in the initial stages of an explosive eruption $Pe \gg 1$ due to fast fragmentation processes. Hence, negligible amounts of gas diffuse into bubbles (Melnik and Sparks, 2002a). We now estimate Pe when the fragmentation front stops.

The diffusion of the gas to the bubbles occurs on a length scale less than the thickness of the shell. The length scale, h_s, is related to the bubble number and gas volume fraction:

$$h_s(\alpha, n) = \frac{3^{1/3}\left(1 - \alpha^{1/3}\right)}{(4\pi n)^{1/3}} \tag{22}$$

We calculate the diffusion time scale for the averaged gas volume fraction α_a in the bubbly liquid with approximation (13):

$$t_D = \frac{\left[h_s(\alpha_a, n_*(1-\alpha_a))\right]^2}{D} \tag{23}$$

We do not consider the diffusion in the zone of gas-particle dispersion, because a parcel of the mixture spends a very short time in this zone compared to the bubbly liquid zone. Consequently, the decompression time t_F is the time for a magma parcel to ascend from its initial position in the chamber or the conduit up to the fragmentation front $t_F = x_f/v_a$, where x_f is the fragmentation front position, v_a is the average velocity of bubbly liquid ascent. The calculations of Melnik and Sparks (2002a, see Fig. 7) provide typical parameters in the conduit in an explosive eruption ($\alpha_a = 0.3$, $x_f = 2$ km, $v_a = 0.1$ m s^{-1}). The ratio between diffusion and ascent time scales is expected to be less than 1 for quasi-static bubble growth:

$$Pe = \frac{3^{2/3}\left(1 - \alpha_a^{1/3}\right)^2 v_a}{(4\pi(1-\alpha_a))^{2/3} x_f} \frac{1}{Dn_*^{2/3}} < 1 \tag{24}$$

For conditions discussed above, the quasi-static model for diffusion will be valid for $Dn_*^{2/3} > 5 \times 10^{-7}$ s^{-1}.

Due to diffusion, there is a distribution of dissolved gas concentration around the bubble and therefore viscosity variation. We average dissolved gas concentration and viscosity in a shell around a bubble for the system of macroscopic Eqs. (1)–(8):

$$c_{av} = \frac{3}{(S^3 - a^3)} \int_a^S r^2 c(r)\mathrm{d}r \tag{25}$$

$$\mu_{av} = \frac{3\theta(\beta)}{(S^3 - a^3)} \int_a^S r^2 \mu(c(r))\mathrm{d}r \tag{26}$$

For crystal contents below 55%, the coefficient is based on the empirical studies of Marsh (1981). For higher crystal contents, the value of the coefficient is quite uncertain, and we follow the estimate of Melnik

and Sparks (1999) based on empirical evidence for very crystal-rich andesite lava domes.

$$\begin{array}{ll} 0\le\beta<0.55 & \theta(\beta)=(1-1.67\beta)^{-2.5} \\ 0.55\le\beta<1 & \log[\theta(\beta)/1.6]=\arctan[20.6(\beta-0.62)]+\pi/2 \end{array} \quad (27)$$

2.4. Fragmentation criteria

For the unsteady model, we study numerically the influence of different fragmentation criteria: threshold gas volume fraction (VF) and threshold overpressure in the bubbles (OP). To investigate the OP criterion, we express the bubble overpressure with the Rayleigh–Lamb equation:

$$\Delta P=\frac{4\mu_{\text{eff}}}{a}\left(\frac{\partial a}{\partial t}+v\frac{\partial a}{\partial x}\right) \quad (28)$$

Here the effective viscosity μ_{eff} represents the integral of the viscous stresses within the shell:

$$\mu_{\text{eff}}=3a^3\varsigma\int_a^S\frac{\mu(c(r))}{r^4}\mathrm{d}r \quad (29)$$

It is calculated according to Lensky et al. (2001). A coefficient ς is included to account for the influence of crystals. The problem here is that individual bubble shells may contain no crystals, but on a larger scale, the expanding system has to deform a crystal-melt mixture. If the crystals have no influence then $\varsigma=1$, but this seems unrealistic for high crystal contents because expanding bubbles have to not only deform the melt shell but contribute to the squeezing of viscous melt around neighbouring crystals on a larger scale. If a bubble is attached to a crystal, it cannot expand easily towards the crystal direction because a crystal undergoes additional resistance from the surrounding melt. Thus, the coefficient ς may be much higher than 1. In our calculations, we take ς equal to $\theta(\beta)$, although ς should be considered as a free parameter since a suitable complicated microscopic model has yet to be developed.

We transform Eq. (28) using Eqs. (1), (2) and (15):

$$\Delta P=\frac{4\mu_{\text{eff}}}{3}\left(\frac{\partial v}{\partial x}+\frac{J}{\rho}\right) \quad (30)$$

The models with two pressures in the mixture by Melnik (2000) show that difference between phase pressures ΔP is small in comparison with the critical overpressure for fragmentation, ΔP_{CR}, in most of the bubbly zone. The value ΔP becomes comparable with ΔP_{CR} only in a small region below the fragmentation front. Therefore, the influence of pressure disequilibrium on mass transfer and gas density remains insignificant and allows to consider conduit flow and bubble growth with one pressure only.

2.5. Approximation for viscosity function

Here we assume that the melt composition is rhyolite and use the experimental results of Hess and Dingwell (1996) for a leucogranite to parameterise the relationship between pure melt viscosity, temperature and water content.

$$\log_{10}\mu(c,T)=0.2911+0.8330\ln c-\frac{1304+2368\ln c}{T-344.2-32.25\ln c} \quad (31)$$

where μ is in Pa s, T is in K, and c is the mass fraction.

The equations for both average and effective viscosities, (26) and (29), contain the pure melt viscosity in the integrals. The integrals have to be calculated at every time step and every grid point, which is very time consuming. In order to increase the code speed, we use a simplified formula in order to get analytical solution for integral expressions.

We found a general approximation of viscosity $\mu_{\text{appr}}(c,T)=A(T)c^{-m(T)}$ where $m(T)$ is an integer and $A(T)$ is a rational function. In the range of 1048 K$<T<$1281 K, the most appropriate approximation μ_{appr} has is:

$$A(T)=\frac{10290-3.545T}{T-195.7}\quad m(T)=3 \quad (32)$$

Fig. 2 compares the Hess and Dingwell formula and the suggested approximation for the temperature $T=1123$ K. In the range $0.01<c<0.05$ the deviation, $\log_{10}\mu(c,T)-\log_{10}\mu_{\text{appr}}(c,T)$, does not exceed 0.36 log units for the parameters in (32).

2.6. Diffusion parameter

We can express bubble number density, bubble and shell radii as functions of α and n_* and put the expressions into the formula for mass transfer (17). An approximate formula for mass flux into the bubble is thus deduced:

$$J=2\left(6\pi^2\right)^{1/3}n^{2/3}D\rho_{\text{m}}^0\frac{\alpha^{1/3}\left(\frac{\rho_{g^*}}{\rho_{m^*}}\alpha+\left(c(a)(1-\alpha)-c_0\frac{n_*}{n}\right)\right)}{3\alpha^{1/3}-\alpha-2} \quad (33)$$

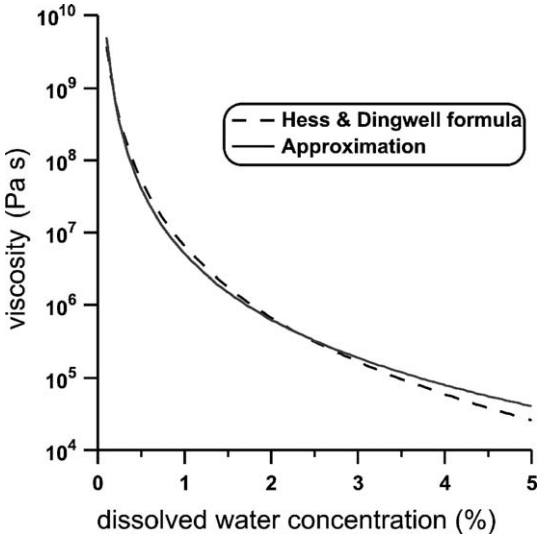

Fig. 2. Comparisons of Hess and Dingwell (1996) formula for viscosity and the approximation used in the model calculations (for a constant temperature, $T=1123$ K).

The integral (11) and its approximation for bubble number density (13) allow us to substitute n/n_*, α and $c(a)$ with ρ/ρ_*, ρ_e/ρ_*, c_0:

$$J = n_*^{2/3} D \rho_m^0 f(\rho/\rho_*, \rho_e/\rho_*, c_0) \tag{34}$$

We can transform the integrals (25), (26) and (29) in the same way. For all the integrals, the terms with n_* disappear, so the effective viscosity and averaged viscosity and concentration do not depend on the diffusion parameters D and n_*. Therefore, Eq. (34) completely presents the contribution of bubble growth dynamics into the flow model. The intensity of mass transfer is controlled by the parameter $\omega = n_*^{2/3} D$ that we call the diffusion parameter. The minimum value of ω was evaluated using Eq. (24). For the maximum possible value of ω, we choose the highest values of n_* observed in nature (Cashman, 2004) and highest diffusivities from water in rhyolitic melts under eruption conditions (Zhang and Behrens, 2000): bubble number density $n_* = 10^{16}$ m^{-3} and diffusion coefficient $D = 10^{-11}$ m^2 s^{-1}. For these values, the diffusion parameter ω is equal to $\omega_{max} = 0.464$ s^{-1} that provides a convenient scale. Below we use the dimensionless diffusion parameter $\varpi = \omega/\omega_{max}$.

3. Boundary and initial conditions

3.1. Steady-state solution

For the slow steady flow in the magma prior to the rapid decompression that initiates explosive activity, the system of governing equations (1–8 has a simplified form

$$\rho v = Q \tag{35}$$

$$\frac{d\rho_e v}{dx} = J \tag{36}$$

$$\frac{dP}{dx} = -\rho g - \frac{32\mu_{av} v}{d^2} \tag{37}$$

Here Q is the extrusion rate per unit area of the conduit cross section. Pressure P, mass flux J and average viscosity μ_{av} are functions of ρ_e and Q. In the modelling of extrusion, we assume a fixed pressure in the chamber P_{ch} at $x=0$, and a fixed pressure at the base of the dome P_{end}, $x=L$. In order to satisfy the boundary conditions, we choose the appropriate value of Q by the shooting method and integrate the system of Eqs. (35)–(37).

3.2. Unsteady solution

For the unsteady explosive flow that develops after a sudden decompression, we solve the transient problem in the conduit of $L+h_d$ length, where h_d is the height of the dome. For the initial conditions for the unsteady model of explosive eruption, we use the corresponding steady-state solution for a extrusion flow over the conduit length of L. We treat the interval above $x=L$ as a gas-particle dispersion zone. A further short length, the height of the dome h_d, is added to the solution above $x=L$ with atmospheric conditions fixed at $x=L+h_d$. This addition gives an initial 'shock' condition at $x=L$. The initial fragmentation front position coincides with the position of the shock.

As the eruption develops, the chamber feeds magma into the conduit. However, for most explosive eruptions, the erupted volume in the initial transient stages is much smaller than the chamber volume; hence, we assume the chamber pressure is fixed. The vesicularity and the viscosity of the magma feeding into the base of the conduit remain constant as well. The pressure at $x=L+h_d$ is fixed to be atmospheric if exit conditions are subsonic; otherwise, for the supersonic regime, no boundary conditions are necessary (Melnik and Sparks, 2002a).

The code used to solve the unsteady problem is based on the Lax–Friedrichs numerical method described in Appendix A.

4. The results

We first present the results for the simulations of extrusion. These simulations will give a possible range

Table 1
Calculation sets

Parameter	Symbol	Values	Dimension
Conduit length	L	5000	m
Pressure at the magma chamber	P_{ch}	130	MPa
Pressure at the base of the dome	P_{end}	5, **10**, 20	MPa
Melt water content	c_0	**0.05**, 0.07	
Conduit diameter	d	30	m
Magma temperature	T_{ch}	1123	K
Magma crystal content	β	0, 0.3, **0.6**	
Gas constant for H_2O	R_w	461	$J \cdot kg^{-1} \cdot K^{-1}$
Density of melt	ρ_m^0	2300	$kg \cdot m^{-3}$
Density of crystals	ρ_x^0	2700	$kg \cdot m^{-3}$
Solubility coefficient	C_f	4.1×10^{-6}	$Pa^{-1/2}$
Diffusion coefficient	D	10^{-12}, $\mathbf{10^{-13}}$, 10^{-14}	$m^2\ s^{-1}$
Number density of bubbles	n_*	10^{10}, $\mathbf{10^{12}}$, 10^{14}	m^{-3}

Bold numbers mark the fixed parameters if not varied.

of initial conditions for the transient problem. Parameters in the steady models (Table 1) were first chosen as appropriate for modelling the eruption of the Soufriere Hills volcano, Montserrat and are typical for a crystal-rich andesite with a rhyolite melt phase. They are mostly taken from Melnik and Sparks (2002a) since we want to compare results with the end member cases considered there. Parameter values marked in bold are those used in calculations unless otherwise specified. We focus on the role of diffusion coefficient D and initial number density of bubbles n_* because the sensitivity of other parameters has been already discussed (Melnik and Sparks, 2002a). Values of n_* were chosen here to represent the wide range of bubble number densities commonly encountered in natural ejecta and lava samples (Mangan and Sisson, 2001). The dimensional analysis establishes that the effect of these parameters can be described by the combination $\omega = n_*^{2/3} D$ and the range of the dimensionless parameter $\varpi = \omega / \omega_{max}$, for values of D and n_* anticipated in nature ϖ is in the interval 2×10^{-6} to 1. We will vary the mass transfer parameter ϖ, changing the number density of bubbles n_* and D within their realistic intervals.

4.1. Initial steady-state profiles

Fig. 3 shows the profiles for averaged dissolved water concentration (a) and gas volume fraction (b) in the conduit below the plug for the case of slow extrusion for $\varpi = 10^{-6}$, 5×10^{-6}, 2×10^{-5}, 5×10^{-4}. At the bottom of the conduit, the magma flow is in equilibrium. The flow stays close to equilibrium as long as its velocity is small and the decompression rate is sufficiently small that mass transfer is close to equilibrium. If the mass transfer parameter ϖ is high and, consequently, the diffusive mass flux is high (see Eq. (34)), the system is maintained close to equilibrium everywhere in the conduit. In Fig. 3 for $\varpi \geq 2 \times 10^{-5}$, the results are close to equilibrium. As ϖ decreases below 2×10^{-5}, the system departs from equilibrium because the bubbles are separated by distances that are greater than the characteristic diffusion distances on the time scale of magma ascent. The concentration of dissolved water becomes larger than the equilibrium concentration at a given pressure (see Fig. 3a). In such circumstances, high supersaturations may develop in regions of the melt far from the bubbles. In such cases, new bubbles may nucleate homogeneously, increasing the number density. According to Mangan et al. (2004), about 100 MPa overpressure has to be reached for homogeneous nu-

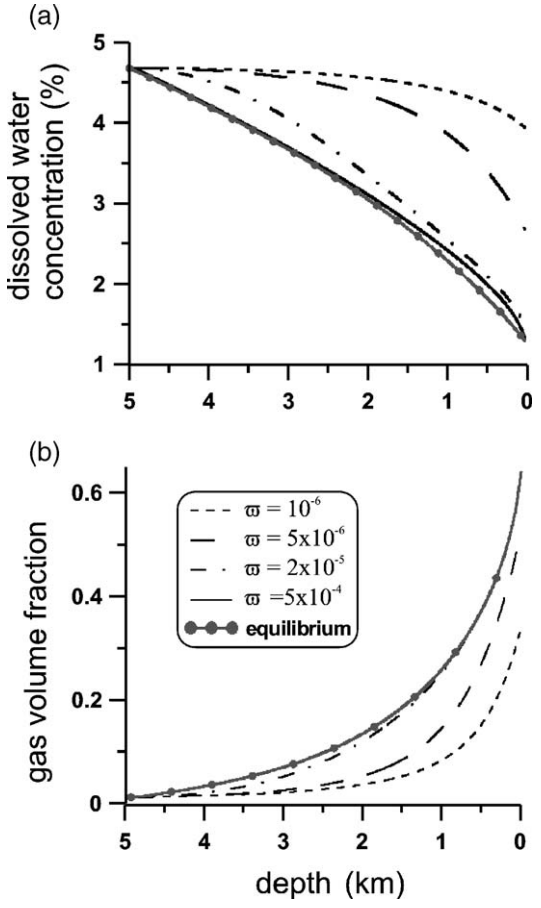

Fig. 3. Distributions of dissolved water concentration (a) and gas volume fraction of bubbles (b) for different values of the mass transfer parameter ϖ in a slow rising column of magma. For larger values of ϖ the system comes close to the equilibrium. Conditions for the calculations are given in Table 1.

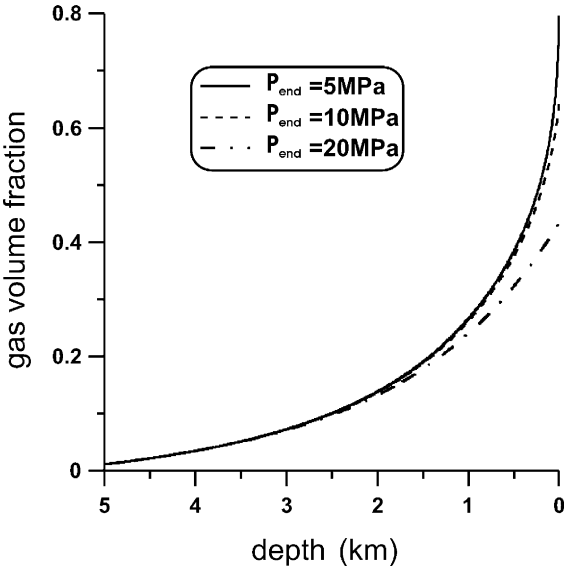

Fig. 4. Distributions of gas volume fraction of bubbles for different confining pressures at the dome in slowly rising magma. Conditions for the calculations are given in Table 1.

cleation that correspond to an oversaturation of about 3 wt.%. Oversaturations calculated in the present results (see Fig. 3a) are smaller (~80 MPa, 2 wt.%) and homogeneous nucleation is not expected. Thus, even in the case of slow extrusion flows, large deviations from equilibrium can occur, on the assumptions of either low bubble number densities or slow diffusion. The gas volume fraction at $x=0$ km determines the vesicularity of the magma at the top of the column which is exposed to a lower pressure by a sudden decompression event. For $\varpi=5\times10^{-4}$, the vesicularity at the top of the column is about 0.6, whereas as a result of disequilibrium, for $\varpi=10^{-6}$, it is about 0.3.

Fig. 4 presents the profiles of gas volume fraction for different dome confining pressures and $\varpi=5\times10^{-5}$. For a confining pressure of about 20 MPa, the top column vesicularity is about 0.4, it tends to 1 as the confining pressure decreases. The difference in the vesicularity of the top of the magma chamber is mostly induced by different values of confining pressure.

Table 2
Calculation sets

Parameter	Symbol	Values	Dimension
Critical gas volume fraction	α_{CR}	0.6	
Critical overpressure	ΔP_{CR}	1	MPa
Dome height	h_d	200	m
Parameters for crystal influence on overpressure	θ	50, **24.2**	

Bold numbers mark the fixed parameters if not varied.

4.2. Transient evolution of eruption

We investigate the transient flow with the VF and OP fragmentation criteria. The discharge rate and fragmentation front evolutions are presented for different sets of parameters (Melnik and Sparks, 2002a). Table 2 contains additional parameters for the unsteady model.

Fig. 5 shows results using the VF criterion. The model with VF fragmentation criterion gives a single eruption pulse. A peak discharge rate is reached after several seconds and then declines gradually. For higher ϖ, the fragmentation front descends deeper and faster. For $\varpi=10^{-6}$, the maximum discharge rate is about 7.5×10^{6} kg·s^{-1}, and for $\varpi=5\times10^{-4}$, it is three times higher. For the larger mass transfer parameter, more gas exsolves from the melt and a magma parcel reaches the fragmentation condition faster. As a consequence, more efficient diffusion influences the frag-

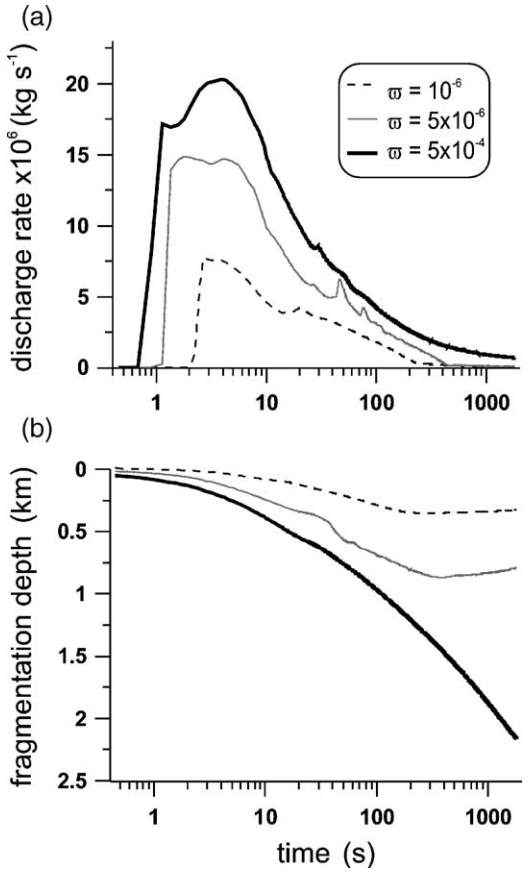

Fig. 5. Variation of discharge rate (a) and fragmentation front position (b) with time for different values of the mass transfer parameter, ϖ, for the volume fraction fragmentation criterion. Conditions for the calculations are given in Tables 1 and 2.

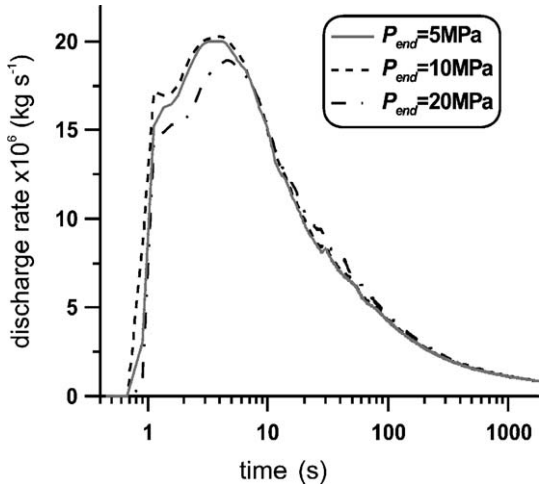

Fig. 6. Variation of discharge rate with time for different confining pressures with VF fragmentation criterion. Although initial gas volume profiles differ significantly (Fig. 4), they do not influence the dynamic of eruption strongly. Conditions for the calculations are given in Tables 1 and 2.

mentation front depth and increases the intensity of discharge.

Fig. 6 shows the discharge rate evolution for different P_{end} from 5 MPa up to 20 MPa. The corresponding initial gas volume profiles are presented on Fig. 4. The wide variation of P_{end} does not influence the peak discharge rate strongly. For higher P_{end} the initial volume fraction of gas is lower and, therefore, the denser mixture cannot accelerate rapidly despite the large pressure drop. Bubble growth in the initial stage of eruption is not efficient due to its very short duration.

The model with OP, criterion given by Eq. (30), produces pulse-like eruptions (Figs. 7 and 8). The fragmentation front falls down in a series of steps. Initially, it travels down with the rarefaction wave after dome collapse. The fragmentation process stops when the overpressure in the bubbles becomes less than the critical value ΔP_{CR}. With no fragmentation, the interface between fragmented and unfragmented magma ascends with the flow. Fragmentation starts again when the critical overpressure is reached and the interface moves downwards. Each fragmentation event induces a pulse in discharge rate.

In Fig. 7, we compare the end member cases, equilibrium and no mass transfer (Melnik and Sparks, 2002a), with our new results using the OP criterion. Our calculation takes into account magma properties that are not considered for the two member cases: diffusion coefficient and bubble number density. In order to represent the influence of these properties, we consider variants of the most and the least intensive mass transfer that might be relevant to natural systems with $\varpi=1$ ($D=10^{-11}$ m^2 s^{-1}, $n_*=10^{16}$ m^{-3}) and $\varpi=2\times10^{-6}$ ($D=10^{-14}$ m^2 s^{-1}, $n_*=10^{12}$ m^{-3}). For comparison with the end member cases, the parameter ς is taken to be equal to 50 as this value was used in Melnik and Sparks (2002a).

There is a little difference in eruptive behaviour over the first 8 s. The first peak in the discharge rate develops in the first several seconds with results being similar for all cases. After about 8 s, the fragmentation fronts evolve differently. For the no-mass-transfer case, the fragmentation front stops at 1.3 km depth and the level of unfragmented magma then tends to return to the initial position. For the equilibrium mass transfer case, fragmentation propagates further down to 2 km and then after a pause descends step by step until reaching the magma chamber. Over a 30-min period, the no-mass-transfer case has only one discharge pulse, the equilibrium mass transfer case has several pulses.

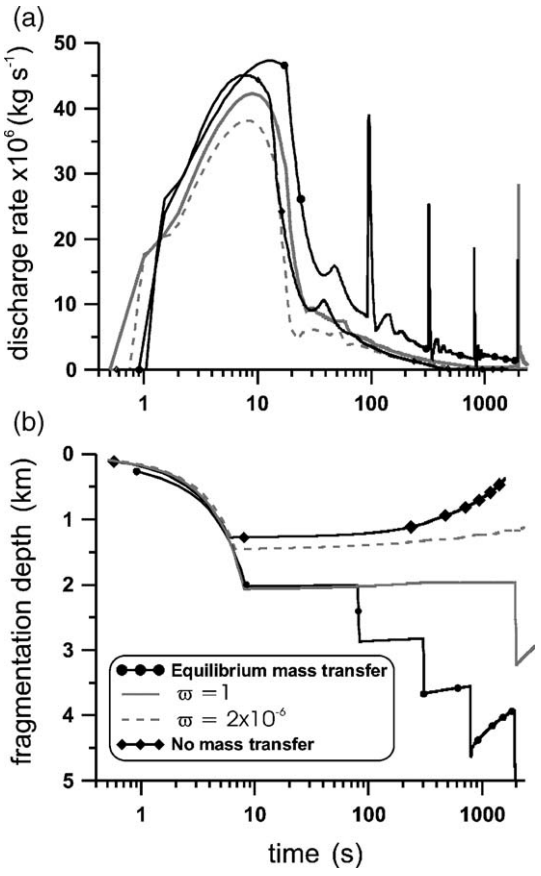

Fig. 7. Variation of discharge rate (a) and fragmentation front position (b) with time for the cases of no mass transfer and equilibrium mass transfer of volatiles and for two cases of disequilibrium mass transfer with overpressure (OP) fragmentation criterion. The last two cases with finite diffusion show intermediate behaviour. Conditions for the calculations are given in Tables 1 and 2.

The new results which take account of mass transfer processes show intermediate behaviour. For the case closer to equilibrium ($\varpi=1$) the fragmentation front stops at 2 km, then the bubbly liquid level rises with the flow over several minutes till the second pulse of fragmentation starts at 33 min. For the case further from equilibrium ($\varpi=2\times10^{-6}$), the fragmentation front descends to 1.5 km depth and then lifts up gradually.

There are major differences between the cases in terms of the mass of magma erupted and in the intensity of eruption. Here we compare results up to 30 min, after which some of the models lose validity due to other effects; for example, as discharge rate falls to very low values, gas leakage from permeable magma may become important so that conditions for explosive flow are no longer achieved. The equilibrium and closer to equilibrium cases last longer and maintain moderately intense discharge rates up to 30 min. They produce significant subsidiary pulses at later stages. As a consequence of their long duration and greater intensity, following the initial peak, much of the magma in the conduit is drained. The models far from equilibrium are much shorter in duration and decline to negligible intensity after 3–5 min. The volume of magma erupted is much smaller and the fragmentation remains at high levels in the conduit. Total masses of erupted material for 30 min are 6.6×10^{9} kg for the equilibrium mass transfer, 3.8×10^{9} kg for $\varpi=1$, 1.6×10^{9} kg for $\varpi=2\times10^{-6}$, 1.6×10^{9} kg for no mass transfer.

Fig. 8 gives results for different initial water concentrations in the melt of $c_0=0.05$, 0.06, 0.07 and a fixed value $\varpi=2\times10^{-4}$. For $c_0=0.07$, the eruption comes to the pulsatory regime in 20 min. The fragmentation front fluctuates at a depth about 3.6 km, producing discharge peaks of about 1.5×10^{7} kg·s^{-1}. The fragmentation front does not reach the magma chamber as in the equilibrium case (see Fig. 7), because the system is still far from equilibrium. The intensity of mass transfer increases due to higher water content, which induces a higher water concentration gradient in the shell around the bubble.

Fig. 9 presents discharge evolution for different crystal contents with a fixed value $\varpi=2\times10^{-4}$. Following Marsh (1981), the corresponding coefficients for viscosity $\theta(\beta)$ are equal to 1 ($\beta=0$) and 5.7 ($\beta=0.3$). In the third case for $\beta=0.6$, we calculate $\theta(\beta)$ with the function developed by Melnik and Sparks (1999), $\theta(0.6)=24.2$. Here, we keep the water content in the melt at the same value so that with decreasing crystal content magma is progressively more water rich. With reducing crystal content, the viscosity decreases. If the viscosity is rather low, the fragmentation front can

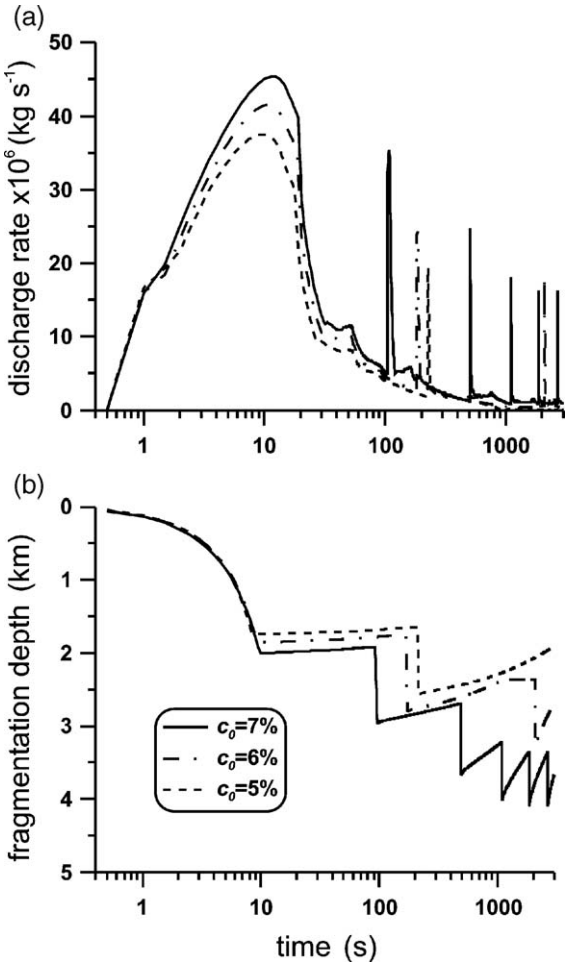

Fig. 8. Variation of discharge rate (a) and fragmentation front position (b) with time for different initial water concentrations c_0 with the OP fragmentation criterion. The system with water-poor magma with the lowest water concentration ($c_0=5\%$) stabilizes to a quasi-steady discharge at long time scales. Conditions for the calculations are detailed in Tables 1 and 2.

temporarily descend lower than a stabilized position before ascending to it. For $\beta=0$, the maximum fragmentation depth reached is about 1.2 km; for $\beta=0.3$, it is about 2.4 km. For $\beta=0.6$, the fragmentation front keeps moving down over the 30 min of the calculation. The stabilized discharges are higher for lower crystal content. These calculations show that an initial transient explosive flow can evolve into a quasi-steady flow with a stabilized fragmentation depth.

Fig. 10 shows the total erupted mass (TEM) for 30 min of eruption via the mass transfer parameter. Two curves correspond to VF (solid curve) and OP (dashed curve) fragmentation criteria. For the minimum mass transfer parameter $\varpi=2\times10^{-6}$ the TEM values are about 1.8×10^{9} kg for VF criterion and 1.6×10^{9} kg

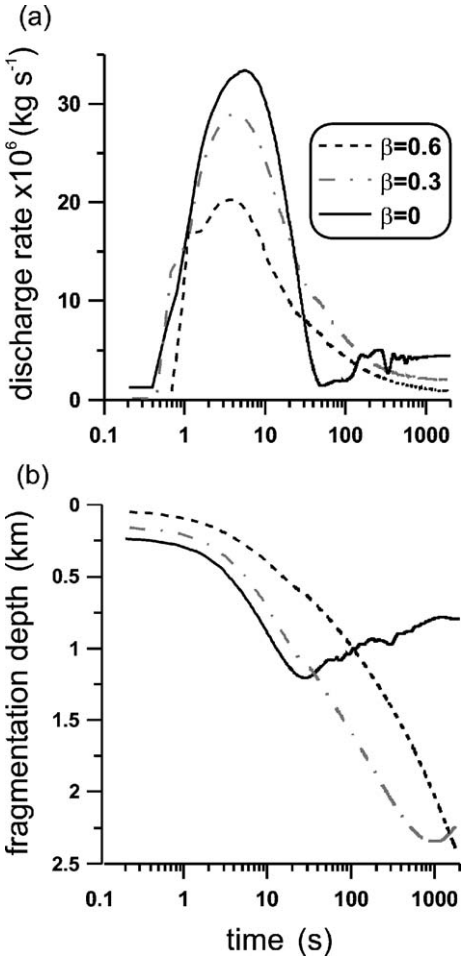

Fig. 9. Variation of discharge rate (a) and fragmentation front position (b) with time for different crystal contents for the VF fragmentation criterion. The crystal-free system shows the highest peak in the discharge rate and re-establishment of eruption at a steady rate of discharge of about 5×10^{6} kg·s^{-1} after nearly ceasing. Conditions for the calculations are given in Tables 1 and 2.

for the OP criterion. For the higher mass transfer parameter, the TEM is higher, because intensity of diffusion helps more material in the conduit to fragment and increase the discharge rate. For the maximum mass transfer parameter $\varpi=1$, the TEM values are about 3.3×10^{9} kg for VF criterion and 3.6×10^{9} kg for OP criterion. For both criteria the curves are close because the most amount of material is erupted in the initial eruption stage due to rarefaction of the volcanic column. Therefore, the TEM may differ by only a factor of 2 due to the mass transfer parameter.

A well-defined parameter set was developed during the "Volcanic Eruption Mechanism Modeling Workshop." The workshop was organized at the University of New Hampshire on November 2002 by Dork Sahagian and Alex Proussevitch. One of the outputs of the workshop was a parameter set used for comparison of different conduit flow models for a sustained explosive eruption of rhyolite magma (Sahagian, 2006). We therefore present the output of the model for this standard set of parameters for rhyolitic magmas (Table 3).

Fig. 11 shows the evolution of discharge and fragmentation front position with the VF criterion ($\alpha_{CR}=0.6$) for the standard set (Table 3) and the standard set modified with different mass transfer parameters: $\varpi=1$ and $\varpi=5\times10^{-5}$. Over about 10 s, the eruptions reach a peak in intensity and then decline. For the case closer to equilibrium, the discharge rate reaches 1.3×10^{8} kg·s^{-1} over 10 s and fragmentation goes down to 3.3 km. For the case closer to disequilibrium, the discharge rate reaches 4.4×10^{7} kg·s^{-1} at 10 s and the fragmentation front goes down to 300 m before lifting up to 80 m depth. If we take lower diffusion coefficient or lower number density of bubbles ($\varpi<5\times10^{-5}$), the system does not reach a threshold condition for fragmentation so an explosive eruption cannot develop. The calculation for the standard set, when diffusion coefficient changes in the interval from 10^{-11} m^2 s^{-1} to 10^{-14} m^2 s^{-1} discharge, lies between these two cases.

For the standard set, the discharge stabilizes at 4.6×10^{7} kg·s^{-1}, and for the close to equilibrium case, the discharge stabilizes at 5.2×10^{7} kg·s^{-1}. These results are in a good agreement with the discharge value of 5.5×10^{7} kg·s^{-1} obtained with the steady model of Melnik et al. (2004) for equilibrium

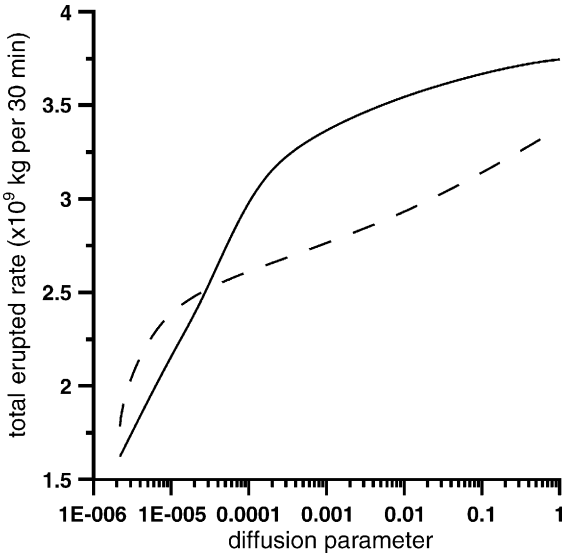

Fig. 10. Variation of total erupted mass (TEM) for 30 min of eruption plotted vs. the mass transfer parameter ϖ for VF criterion (solid curve) and OP fragmentation criterion (dashed curve). Conditions for the calculations are detailed in Tables 1 and 2.

Table 3
Standard set for rhyolitic magma

Parameter	Symbol	Values	Dimension
Conduit length	L	8	km
Pressure at the magma chamber	P_{ch}	200	MPa
Pressure at the base of the dome	P_{end}	10	MPa
Melt water content	c_0	0.0585	
Conduit diameter	d	50	m
Magma temperature	T_{ch}	1123	K
Magma crystal content	β	0	
Gas constant for H_20	R	461	$J \cdot kg^{-1} \cdot K^{-1}$
Density of melt	ρ_m	2200	$kg \cdot m^{-3}$
Density of crystals	ρ_x	2700	$kg \cdot m^{-3}$
Solubility coefficient	C_f	3.47×10^{-6}	$Pa^{-1/2}$
Diffusion coefficient	D	Zhang formula (Zhang and Behrens, 2000)	$m^2\ s^{-1}$
Number density of bubbles in the chamber	n_0	10^{15}	m^{-3}
Critical gas volume fraction	α_{CR}	0.6	

conditions. The low discharges in all of the illustrative cases reflect the effects of disequilibrium.

An important result, illustrated in both Figs. 9 and 11, is that in certain parameter ranges the systems stabilize at a definite depth with a high discharge rate. This stabilization represents the establishment of a sustained quasi-steady explosive eruption, which then lasts for many hours or days provided an appropriate volume of magma exists. Our results thus display two kinds of transient behaviour: eruptions which decline to negligible intensity and are expected to stop, and eruptions that stabilize at a high intensity and become sustained.

5. Discussion

Our modelling is related to some fundamental issues of the variety of eruptive styles at explosive volcanoes. Here we focus on the controls on the duration of explosive eruptions with the behavioural extremes being very short-lived, albeit intensive, Vulcanian explosions and long-lived sustained Plinian eruptions. Our discussion uses the recent eruptions of Mount St. Helens, Pinatubo, Soufriere Hills, Montserrat and Lascar, Chile, as examples of various behaviours.

We start by considering the case of short-lived Vulcanian explosions which alternate with dome-growth activity, as is observed at Soufriere Hills, Montserrat (Druitt et al., 2002), Lascar (Matthews et al., 1997), and Pinatubo prior to the climactic eruption (Delinger and Hoblitt, 1999). Such Vulcanian explosions are very short-lived (a few tens of seconds) and the volumes erupted are only commensurate with emptying of the upper parts of the conduit (Druitt et al., 2002). Dome growth can resume shortly after Vulcanian explosions. Our results confirm that such explosions can occur under disequilibrium conditions with the fragmentation level never reaching deep into the conduit and the most intense peak in activity occurring in the first 10–30 s, after which flow rates fall to negligible values in a few hundred seconds.

We suggest that the principal processes causing the explosive flow to stop are permeability development in the magma and weak diffusion. Once fragmentation stops, gas escape through permeable magma may prevent the resumption of fragmentation. Here we consider this process only qualitatively. The critical control is whether the bubble pressure increases due to decompression or decreases due to gas escape through permeable magma. In the high-intensity first pulse

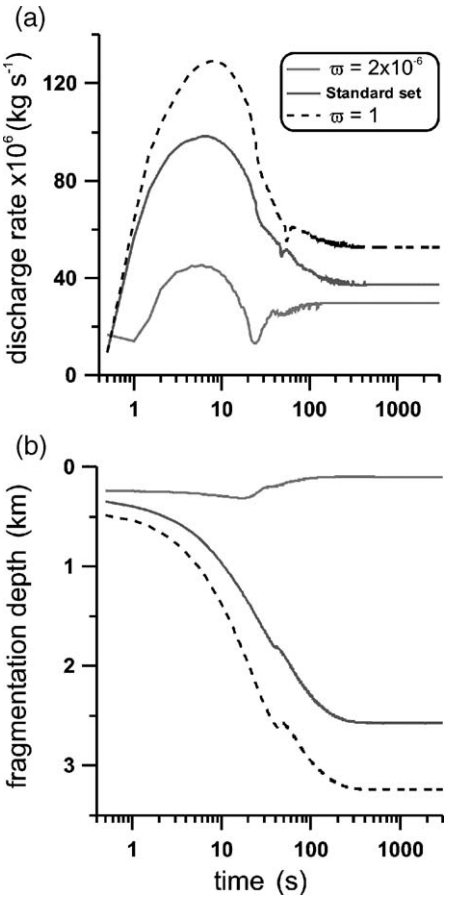

Fig. 11. Variation of discharge and fragmentation front position with time for the cases of no mass transfer and equilibrium mass transfer of volatiles and for two cases of disequilibrium mass transfer with VF fragmentation criterion. The last two cases have intermediate behaviour. Conditions for the calculations are detailed in Table 3.

decompression is the dominant factor so the overpressures build up; gas escape by permeable flow is negligible. However, as the intensity and decompression rate decline, a time is reached when permeable gas escape becomes dominant so overpressure can no longer develop. It is indeed plausible that the foam starts to collapse to reconstitute bubbly magma into dense magma. This later process may also have a role in stopping further explosive activity since the strength of magma and fragmentation threshold greatly increase as porosity decreases (Spieler et al., 2004). The concept is supported by observations on Montserrat where strong ash-venting and seismic tremor occur for tens of minutes following Vulcanian explosions (Druitt et al., 2002). This strong degassing is also accompanied by deflation as recorded by tilt meter (Voight et al., 1999) and observations of slow rise of degassed magma in the conduit in the following hours.

An intermediate style of activity between the Vulcanian and sustained Plinian eruptions can be deduced from observations at Soufriere Hills and Mount St. Helens. On September 1996 at Soufriere Hills, a sub-Plinian explosive eruption occurred for a period of about 50 min, following a major episode of a dome collapse (Robertson et al., 1998). After the climactic eruption of 18 May 1980 at Mount St Helens, there were several episodes of sub-Plinian eruptions in the following months of 1980. Each explosive eruption lasted a few tens of minutes and was then followed by episodes of dome growth lasting a few days (Swanson and Holcomb, 1989). We suggest that this style of eruption corresponds to cases where the magma properties and conditions were closer to equilibrium so that the explosive eruption could reach to greater depths in the conduit and could be sustained at higher intensities for significantly longer. Our models show that a system that can be maintained closer to equilibrium has the attributes of such sub-Plinian events associated with dome growth. Observations indicate that the sub-Plinian eruptions of September 1996 at Soufriere Hills reached depths of 3–4 km (Robertson et al., 1998). This eruption was also characterized by several short seismic pulses which Melnik and Sparks (2002a) interpreted as corresponding to the strong secondary pulses predicted in the models. Such eruptions may also cease and activity transform to dome extrusion, because the intensity declines to the point where gas escape becomes important and overpressures required for further explosive activity can no longer be attained.

The other end member style of explosive eruptions are Plinian eruptions that can last several hours, involve large volumes of magma and high intensities and can be sustained or even increase with time. From a hazard point of view, it is important to understand what the critical factors are that allow such a sustained explosive eruption to develop. The size of the magmatic system cannot be a factor, for example. It is now clear that the Soufriere Hills chamber is substantial with over 0.5 km^3 of magma erupted so far, but conditions for a sustained eruption have never developed in this system. The Vulcanian events and single sub-Plinian event on Montserrat never evolved into sustained eruptions. At Pinatubo, there was an earlier episode of short-lived explosive eruptions alternating with dome growth, which led into a major Plinian eruption. In contrast, at Mount St. Helens the sustained Plinian eruption of 18 May 1980 occurred early and later the system only being capable of short-lived sub-Plinian explosive eruptions alternating with lava dome growth.

Our model sheds some light on these matters. We have established that magma viscosity and water content may be important factors. By varying the crystal content, we could model eruptions that evolve quasi-steady states with a balance between magma flow from the chamber into the conduit and outflow into the dispersion zone with the fragmentation level being at the stationary location in the conduit. In this case, fragmentation never ceases and conditions for sustained discharge are achieved. The controlling parameters that favour establishing of such conditions are relatively low magma viscosity in the deep parts of the conduit, which allows an adequate supply of fresh magma, so that flow rate does not drop to negligible values and gas escape through permeable magma never becomes important in suppressing and stopping explosive activity.

At least qualitatively, these interpretations based on modelling results are consistent with observations at the various case study volcanoes. For Montserrat, the andesite magma is very phenocryst rich (Murphy et al., 2000) and so has an unusually high viscosity and low bulk water content (~2.0–2.5% H_2O). We suggest at Montserrat that the initial unsteady explosive flows always decline to very low intensity where fragmentation stops and gas escape becomes dominant, killing off the possibility of sustained explosive eruption developing. At Mount St. Helens, conditions were appropriate for more sustained discharge because gas-rich and sufficiently low viscosity magma had intruded at a high crustal level. After explosive disruption of the cryptodome, a sustained explosive eruption was able to develop so that a significant volume

of the magma chamber (~0.2 km^3) was expelled. We suggest that following the climactic eruption, the chamber viscosity increased significantly, perhaps due to the combination of crystallization and gas loss resulting from the 18 May 1980 eruption. This possibility is supported by the petrological observations of higher crystallinities in later products of this eruption (Cashman, 1992; Blundy and Cashman, 2001). Combination of parameters in the post-18 May system never allowed conditions for sustained Plinian-style eruption to develop again.

There remain several unresolved issues and clear opportunity for further model development. One of the strong controls on the models is the bubble number density which we have used as a free parameter. This parameter has an important role in controlling how far from equilibrium the system can get. Our model is also simplified by only having a single nucleation event. Thus, although the models span parameter ranges that seem reasonable for most magmatic systems, the time history of bubbles nucleation is not included. It could well be that some of the models explored are not realized in nature simply because physical conditions either prevent or allow high nucleation rates and bubble densities. Future models will need to incorporate nucleation kinetics to identify which scenarios are realistic.

In general, we can state the following on the basis of present understanding of nucleation. High crystal content magmas may favour heterogeneous nucleation and high bubble densities, especially if large numbers of microlites are formed. High bubble density in its turn favours development of magma permeability, bubble coalescence and high viscosity, all of which are factors that tend to inhibit explosive eruption at shallow levels, by allowing gas to escape. Very large supersaturation of 70–140 MPa are required to cause homogenous nucleation in melts (Hurwitz and Navon, 1994; Mangan and Sisson, 2001). In a crystal-poor magma, those values can be achieved even during weak heterogeneous nucleation. Then intensive homogeneous nucleation takes place and results in very high bubble number densities. Above the nucleation threshold, magma can be maintained close to equilibrium. The low viscosity of crystal-poor magmas favours rapid inflow and supply to the conduit from chambers. In general, therefore, crystal-poor gas-rich magmas favour Plinian style eruptions. For crystal-rich magmas, the bubble nucleation level that is expected to be deep and large supersaturations are more difficult to develop during slow magma ascent. Bubble number density will be determined by the crystal number density and can be expected to be quite low (10^9–10^{11} m^{-3}). During slow ascent, the crystal-rich magmas can still maintain equilibrium or can be closer to the equilibrium but can be expected to be far from equilibrium at the onset of explosive activity. The combination of high viscosity in crystal-rich magmas and preexisting bubbles at depth favour Vulcanian and sub-Plinian style eruptions.

Present models of magma flow are ready to incorporate the development of magma permeability as well as nucleation kinetics. It seems likely that permeability is a critical factor in determining whether an eruption evolves into a sustained Plinian event that can erupt a significant proportion of a chamber or is characterized by short-lived explosions and lava dome growth. Unfortunately, the processes of bubble nucleation and coalescence are still not sufficiently well understood to be incorporated quantitatively into models, although simplified models can be developed with plausible parameterizations of the processes.

6. Conclusion

Our model simulations indicate that mass transfer processes are likely to play an important role in determining eruptive style. Our study has focused on the initial unsteady stages of an explosive eruption following a triggering event that suddenly causes a large pressure drop in a column of magma. The models simulate a range of behaviours from short-lived but intense explosions lasting just a few tens of seconds, to longer eruptions which can last tens of minutes, but eventually decline to negligible flow rates, to those eruptions that evolve into quasi-steady sustained eruptions and might last hours or even days. Comparable behaviours can be deduced from the observations of different styles from Vulcanian explosions to more prolonged eruptions which decline in intensity after an initial peak to long-lived sustained explosive eruptions. The model supports the proposal of Melnik and Sparks (2002a) that this spectrum of behaviours represents conditions in the eruptive system that range from near disequilibrium to those that are close to equilibrium.

For the parameters chosen in this study, eruptive conditions never quite reach the end-member situations. The extent of disequilibrium is principally governed by a parameter, $\omega = n_*^{2/3} D$, which is a measure of efficiency of mass transfer and by a range of parameters that offset the time-scales of magma flow and decompression. Factors that favour

short Vulcanian eruptions include low bubble densities, low gas diffusivity, low dissolved water concentration and high magma viscosity induced by high crystal content. Factors that favour the development of sustained explosive eruptions include high bubble densities, high magma gas diffusivity, high dissolved water concentration and low magma viscosity. In addition, development of magma permeability, allowing gas escape, is identified as a key process (Jaupart and Allegre, 1991). Under such conditions gas escape through permeable magma may prevent the system moving back to explosive conditions and thus explain why dome growth can resume. For the sustained case, flow rates and fragmentation rates never decrease sufficiently for gas escape to become important.

Acknowledgements

This work was supported by the NERC Grant (GR3/13020), INTAS grant (01-106), and MULTIMO EC Research Project (EVGI-2000-00574). RSJS was supported by a Royal Society-Wolfson Merit Award. The authors thanks Larry Mastin and Alex Proussevitch for helpful reviews.

Appendix A. Numerical Technique

The Lax-Friedrichs conservative method (Guang-Shan and Tadmor, 1998) is applied for unsteady flow in the conduit. We use it since our system of Eqs. (1–5) can be represented in the conservative form

$$\frac{\partial u}{\partial t}+\frac{\partial f(u)}{\partial x}=\psi(u,t)$$

$$u=(\rho,\rho_e,Q)\quad Q=\rho v$$

$$f(u)=\left(Q,\rho_e v,P+\rho v^2\right)$$

$$\psi=\left(0,J,-\rho g-\lambda\frac{32\mu_{av}}{d^2}v\right) \tag{38}$$

The method works on the equally spaced x-grid with step Δx. We chose time step Δt_n to satisfy CFL conditions (Guang-Shan and Tadmor, 1998). The x-grid has to be staggered on $0.5\Delta x$ on the odd time step Δt_n: $x_i^n=x_i^{n+1}+.5\Delta x$. At any time step, the vector function $u(x)$ is fitted by a piecewise-linear approximation. In order to account for discontinuities we use the Minmod function, which chooses the best appropriate slope $u'_i(x_i^n,t_n)$ from numerical derivatives for the approximation:

$$\mathrm{Minmod}(d_1,d_2,d_3)=\begin{cases}0 & \exists k,l: d_k d_l\le 0\\ \min_i(d_i) & \forall k\ d_k<0\\ \max_i(d_i) & \forall k\ d_k>0\end{cases} \tag{39}$$

Here, instead of parameters d_i left, right, and central derivatives are substituted. The principal method formulas follow from the approximation of Eq. (38) in the integral form on the rectangle $\{(x_i^n,t_n),\ (x_i^n+\Delta x,t_n),\ (x_i^n,t_{n+1}),\ (x_i^n+\Delta x,t_{n+1})\}$. The method has two semi-steps: predictor that approximate the values $u(x_i^n,t_n+0.5\Delta t_n)$, and corrector that calculates the values $u(x_i^n+.5\Delta x,t_{n+1})$ on the staggered grid.

$$u(x_i,t_n+.5\Delta t_n)u(x_i,t_n)+\frac{\Delta t_n}{\Delta x}f'(u(x_i,t_n))$$

$$u(x_i+.5\Delta x,t_{n+1})\approx\frac{1}{2}(u(x_i,t_n)+u(x_{i+1},t_n))+\frac{1}{8}(u'(x_i,t_n)-u'(x_{i+1},t_n))+\frac{\Delta t_k}{\Delta x}(f(u(x_{i+1},t_n+.5\Delta t_n))-f(u(x_i,t_n+.5\Delta t_n))) \tag{40}$$

To estimate the accuracy of this method, the transient task was solved until stabilization and stabilized profiles were compared with profiles from the steady-state solution that was solved by the integration of ODE. For 500 cells in the x-grid, the steady and stabilized pressure profiles coincide up to 0.1%.

Appendix B. Boundary conditions

The LxF method deals with staggered grid that requires special treatment of boundary conditions. If the scheme executes on an odd time step, two vectors have to be calculated additionally for the next step: $u(0,t_k)$ and $u(L,t_k)$; after an even time step four vectors have to be calculated $u(-.5\Delta x,t_k)$, $u(.5\Delta x,t_k)$, $u(L-.5\Delta x,t_k)$, and $u(L+.5\Delta x,t_k)$. To obtain these values, we make the linear projections of pressure, gas volume and discharge fraction and restore vectors u on the boundaries accordingly to Eqs. (4–7), (11),

(12). As pressure in the chamber (P_{ch}) is fixed, we make projection with boundary data:

$$k = 2z \qquad P(.5\Delta x, t_k) = \frac{1}{3}P(1.5\Delta x, t_k) + \frac{2}{3}P_{ch}$$
$$P(-.5\Delta x, t_k) = 2P_{ch} - P(.5\Delta x, t_k)$$

$$k = 2z+1 \qquad P(0, t_k) = P_{ch} \tag{41}$$

As the discharge is not fixed at the boundaries, its linear projection is built with its closest known values. To avoid disturbances from the upper boundary conditions the initial grid was enlarged with additional ghost cells. The numerical technique greatly differs from the one applied in Melnik and Sparks (2002a, see Appendix) and, unfortunately, it hampers the precise congruence of the variants presented in Fig. 7 that has to take place in the first seconds of eruption.

References

Barmin, A.A., Melnik, O.E., 1993. Features of eruption dynamics of high viscosity gas-saturated magmas. Fluid Dynamics 2, 49–57.

Blundy, J., Cashman, K.V., 2001. Ascent-driven crystallization of dacite magmas at Mount St. Helens, 1980–1986. Contributions to Mineralogy and Petrology 140, 631–651.

Cashman, K.V., 1992. Groundmass crystallization of Mount St. Helens dacite, 1980–1986: a tool for interpreting shallow magmatic processes. Contributions to Mineralogy and Petrology 109, 431–449.

Cashman, K.V., 2004. Volatile control on magma ascent and eruption. Monograph of the American Geophysical Union. In: Sparks, R.S.J., Hawhesworth, C.J. (Eds.), State of the Planet: Frontiers and Challenges.

Delinger, R.P., Hoblitt, R.P., 1999. Cyclic eruptive behavior of silicic volcanoes. Geology 27, 459–462.

Dobran, F., 1992. Non-equilibrium flow in volcanic conduits and application to the eruptions of Mt. St. Helens on May 18, 1980, and Vesuvius in AD 79. Journal of Volcanology and Geothermal Research 49, 285–311.

Druitt, T.H., Young, S., Baptie, B., Calder, E., Clarke, A., Cole, P., Harford, C., Herd, R., Luckett, R., Ryan, G., Sparks, S., Voight, B., 2002. Episodes of cyclic Vulcanian explosive activity with fountain collapse at Soufriere Hills volcano, Montserrat. In: Druitt, T.H., Kokelaar, B.P. (Eds.), The Eruption of Soufriere Hills Volcano, Montserrat, from 1995 to 1999, Memoirs of the Geological Society of London, vol. 21, pp. 281–306.

Gardner, J.E., Hilton, M., Carroll, M.R., 2000. Bubble growth in highly viscous silicate melts during continuous decompression from high pressure. Geochimica et Cosmochimica Acta 64, 1473–1483.

Guang-Shan, J., Tadmor, E., 1998. Non-oscillatory central schemes for multidimensional hyperbolic conservation laws. Journal of Scientific Computing 19, 1892–1917.

Hess, K.U., Dingwell, D.B., 1996. Viscosities of hydrous leucogranitic melts: a non-Arrhenian model. American Mineralogist 81, 1297–1300.

Hurwitz, S., Navon, O., 1994. Bubble nucleation in rhyolitic melts: experiments at high pressure, temperature, and water content. Earth and Planetary Science Letters 122, 267–280.

Jaupart, C., 1998. Gas loss from magmas through conduit walls during eruptions. In: Gilbert, G.S., Sparks, R.S.J. (Eds.), Physics of Explosive Eruptions, Special Publication-Geological Society of London, vol. 145, pp. 27–50.

Jaupart, C., Allegre, C.J., 1991. Gas content, eruption rate and instabilities of eruption regime in silicic volcanos. Earth and Planetary Science Letters 102, 413–429.

Lensky, N.G., Lyakhovsky, V., Navon, O., 2001. Radial variations of melt viscosity around growing bubbles and gas overpressure in vesiculating magmas. Earth and Planetary Science Letters 186, 1–6.

Mangan, M., Sisson, T., 2001. The influence of bubble nucleation mechanism on eruptive degassing: experiments with dacite and rhyolite melts. EOS 82.

Mangan, M., Mastin, L., Sisson, T., 2004. Gas evolution in eruptive conduits: combining insights from high temperature and pressure decompression experiments with steady-state flow modeling. Journal of Volcanology and Geothermal Research 129, 23–36.

Marsh, B.D., 1981. On crystallinity, probability of occurrence and rheology of lava and magma. Contributions to Mineralogy and Petrology 78, 85–98.

Matthews, S.J., Gardeweg, M.C., Sparks, R.S.J., 1997. The 1984 to 1996 cyclic activity of Lascar Volcano, Northern Chile; cycles of lava dome growth, dome subsidence, degassing and explosive eruptions. Bulletin of Volcanology 59, 72–82.

Melnik, O., 2000. Dynamics of two-phase conduit flow of high-viscosity gas-saturated magma: large variations of sustained explosive eruption intensity. Bulletin of Volcanology 62 (3), 153–170.

Melnik, O.E., Sparks, R.S.J., 1999. Nonlinear dynamics of lava dome extrusion. Nature 402, 37–41.

Melnik, O.E., Sparks, R.S.J., 2002a. Modelling of conduit flow dynamic during explosive activity at Soufriere Hills Volcano, Montserrat. In: Druitt, T.H., Kokelaar, B.P. (Eds.), The Eruption of Soufriere Hills Volcano, Montserrat, from 1995 to 1999, Memoirs of the Geological Society of London, vol. 21, pp. 307–317.

Melnik, O.E., Sparks, R.S.J., 2002b. The dynamics of magma ascent and lava extrusion at the Soufriere Hills Volcano, Montserrat. In: Druitt, T.H., Kokelaar, B.P. (Eds.), The Eruption of Soufriere Hills Volcano, Montserrat, from 1995 to 1999, Memoirs of the Geological Society of London, vol. 21, pp. 153–171.

Melnik, O.E., Barmin, A.A., Sparks, R.S.J., 2004. Conduit flow model for the case of high-viscous, gas-saturated magma. Journal of Volcanology and Geothermal Research 143, 53–68.

Murphy, M.D., Sparks, R.S.J., Barclay, J., Carroll, M.R., Brewer, T.S., 2000. Remobilization of andesite magma by intrusion of mafic magma at the Soufriere Hills volcano, Montserrat, West Indies. Journal of Petrology 41, 21–42.

Navon, O., Lyakhovsky, V., 1998. Vesiculation processes in the silic magmas. In: Gilbert, G.S., Sparks, R.S.J. (Eds.), Physics of Explosive Eruptions, Special Publication-Geological Society of London, vol. 145, pp. 27–50.

Papale, P., 1999. Numerical simulations of magma ascent along volcanic conduits. Physics and Chemistry of the Earth 24, 957–961.

Papale, P., Dobran, F., 1993. Modeling of the ascent of magma during the Plinian eruption of Vesuvius in A.D. 79. Journal of Volcanology and Geothermal Research 58, 101–132.

Proussevitch, A.A., Sahagian, D.L., 1996. Dynamics of coupled diffusive and decompressive bubble growth in magmatic systems. Journal of Geophysical Research 101 (17), 447–517.

Proussevitch, A.A., Sahagian, D.L., Anderson, A.T., 1993. Dynamics of diffusive bubble growth in magmas: isothermal case. Journal of Geophysical Research 98 (22), 283–307.

Robertson, R.E.A., Cole, P., Sparks, R.S.J., Harford, C.L., Lejeune, A.-M., McGuire, W.J., Miller, A.D., Murphy, M.D., Norton, G., Stevens, N.F., MVO Team, 1998. The explosive eruption of Soufriere Hills Volcano, Montserrat September 17, 1996. Geophysical Research Letters 25, 3429–3432.

Sahagian, D., 2006. Volcanic eruption mechanisms: insights from intercomparison of models of conduit processes. Journal of Volcanology and Geothermal Research 143, 1–15.

Slezin, Yu.B., 2003. The mechanism of volcanic eruptions (a steady state approach). Journal of Volcanology and Geothermal Research 122, 7–50.

Sparks, R.S.J., 1978. The dynamics of bubble formation and growth in magmas: a review and analysis. Journal of Volcanology and Geothermal Research 3, 1–37.

Spieler, O., Dingwell, D.B., Alidibirov, M., 2004. Magma fragmentation speed: an experimental determination. Journal of Volcanology and Geothermal Research 129, 109–123.

Stasiuk, M.V., Jaupart, C., 1997. Lava flow shapes and dimensions as reflections of magma system conditions. Journal of Volcanology and Geothermal Research 78, 31–50.

Swanson, D.A., Holcomb, R.T., 1989. Regularities in growth of the Mount St. Helens dacite dome, 1980–1986. IAVCEI Proceedings in Volcanology, 1.2, Lava Flows and Domes. Springer-Verlag, pp. 3–24.

Taylor, B.E., Eichelberger, J.C., Westrich, H.R., 1983. Hydrogen isotopic evidence of rhyolitic magma degassing during shallow intrusion and eruption. Nature 306, 541–545.

Voight, B., Glicken, H., Janda, R.J., Douglas, P.M., 1981. Catastrophic rock-slide avalanche of May 18. U.S. Geological Survey Professional Paper 1250, 347–377.

Voight, B., Sparks, R.S.J., Miller, A.D., Stewart, R.C., Hoblitt, R.P., Clarke, A., Ewart, J., Aspinall, W., Baptie, B., Druitt, T.H., Herd, R., Jackson, P., Lockhart, A.B., Loughlin, S.C., Lynch, L., McMahon, J., Norton, G.E., Robertson, R., Watson, I.M., Young, S.R., 1999. Magma flow instability and cyclic activity at Soufriere Hills Volcano, Montserrat. B.W.I. Science 283, 1138–1142.

Wilson, L., Sparks, R.S.J., Walker, G.P.L., 1980. Explosive volcanic eruptions—IV. The control of magma properties and conduit geometry on eruption column behaviour. Geophysical Journal of the Royal Astronomical Society 63, 117–148.

Woods, A.W., Koyaguchi, T., 1994. Transitions between explosive and effusive eruptions of silicic magmas. Nature 370, 641–644.

Zhang, Y., Behrens, H., 2000. H_2O diffusion in rhyolitic melts and glasses. Chemical Geology 169, 243–262.